Journal Pre-proof

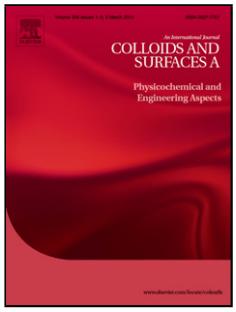

Unveiling the hydrogen bonding network in liquid crystalline natural-based glycosides containing polymeric complexes: experimental and theoretical assessment

Nurul Fadhilah Kamalul Aripin (Conceptualization) (Data curation) (Writing - original draft) (Writing - review and editing) (Funding acquisition), Jonathan Heap (Data curation) (Formal analysis), Rafael Piñol (Data curation) (Methodology), Vijayan M. Achari (Data curation) (Formal analysis) (Writing - original draft), Alfonso Martinez-Felipe (Conceptualization) (Investigation) (Writing - original draft) (Writing - review and editing) (Funding acquisition)

PII: S0927-7757(20)30278-8

DOI: https://doi.org/10.1016/j.colsurfa.2020.124685

Reference: COLSUA 124685

To appear in: *Colloids and Surfaces A: Physicochemical and Engineering Aspects*

Received Date: 13 December 2019

Revised Date: 27 February 2020

Accepted Date: 10 March 2020

Please cite this article as: Kamalul Aripin NF, Heap J, Piñol R, Achari VM, Martinez-Felipe A, Unveiling the hydrogen bonding network in liquid crystalline natural-based glycosides containing polymeric complexes: experimental and theoretical assessment, *Colloids and Surfaces A: Physicochemical and Engineering Aspects* (2020), doi: https://doi.org/10.1016/j.colsurfa.2020.124685

Unveiling the hydrogen bonding network in liquid crystalline natural-based glycosides containing polymeric complexes: experimental and theoretical assessment.

Nurul Fadhilah Kamalul Aripin[1,2], Jonathan Heap[3], Rafael Piñol[4], Vijayan M. Achari[2,5], Alfonso Martinez-Felipe[3,*]

[1]Faculty of Chemical Engineering, Universiti Teknologi MARA, 40450 Shah Alam, Selangor Darul Ehsan, Malaysia.

[2]Fundamental and Frontier Sciences in Nanostructure Self-Assembly Center, Department of Chemistry, Faculty of Science, University of Malaya, 50603 Kuala Lumpur, Malaysia.

[3]Chemical and Materials Engineering Group, School of Engineering, University of Aberdeen, King's College, Aberdeen AB24 3UE, Scotland, UK.

[4]Department of Condensed Matter Physics and Aragon Materials Science Institute, ICMA, University of Zaragoza- CSIC, Zaragoza, 50009 Spain.

[5]Bioinformatics Program, Institute of Biological Sciences, Faculty of Science, University of Malaya, 50603 Kuala Lumpur, Malaysia.

Graphical abstract

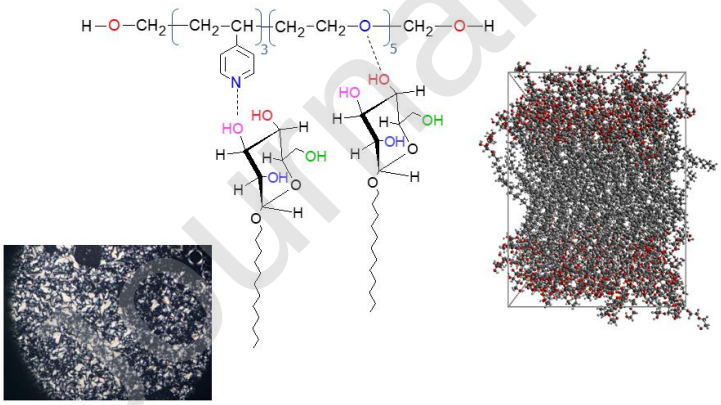

Abstract

In this work we present a facile and versatile strategy to prepare new amphiphilic compounds obtained from natural sources, avoiding costly covalent synthetic stages, and we introduce a

powerful methodology to describe hydrogen-bonding networks in carbohydrates liquid crystal. A series of new glycosides has been prepared by mixing a natural-based mannoside, αManPKO, with three different polymeric substrates: poly(ethylene oxide), PEG, poly(4-vinyl pyridine), P4VP, and a block-copolymer containing PEG and P4VP segments, PEG_{45}-*b*-$P4VP_{18}$. The materials have been characterised by differential scanning calorimetry, polarised optical microscopy and small-angle X-ray diffraction. The resulting complexes are assembled by hydrogen-bonding and form smectic A phases, with the polymeric chains spread along the surface of the glycosides bilayers. By using Fourier-transform infrared spectroscopy, FT-IR, and molecular simulations, we have assessed the selectivity of the hydrogen bonds formed between αManPKO and the polymeric segments. Our results suggest that the assembly of the polymeric complexes must be explained by a combination of interfacial mixing between the polymer/glycoside units at the bilayer boundaries (favoured by PEG) and the formation of strong hydrogen bonds (favoured by P4VP).

Keywords: Glycosides, supramolecular liquid crystals, hydrogen bonding, Fourier-transform infrared spectroscopy, polymeric complexes, molecular simulation.

1. Introduction

Hydrogen-bonding is a versatile technique to yield new supramolecular liquid crystals [1, 2], thanks to the directional character of the hydrogen bonds that facilitates the arrangement of anisotropic structures. The typical strength of a hydrogen bond (1∼60 $kJ \cdot mol^{-1}$) [3, 4] can guarantee the stability of the new materials above their processing melting points, whilst providing some degree of "softness". Some early examples of complexes with mesogenic character include the pyridine-benzoic assemblies, reported by Kato and co-workers[5, 6], or the seminal works by Bruce and co-workers, using alkoxystilbazoles.[7-9] To date, a wide range of liquid crystals continues to be prepared by hydrogen-bonding, including, chiral bent-core with supramolecular induced chirality [10, 11], photosensitive liquid crystals[12, 13], modular assemblies showing broad blue phases[14], supramolecular dimers exhibiting the twist-bend nematic phase [15-17], or smectic networks for selective mass and ionic transport [18-20], among many others.

Carbohydrate liquid crystals can be considered as early precedents of supramolecular mesomorphic compounds, and were already reported in the first half of the 20th century[21, 22]. More specifically, the different hydroxyl groups can form multiple hydrogen bonds between glycosides, resulting in microphase separation between polar and non-polar regions, and ultimately favouring smectic behaviour [23-29]. We note, however, that the exhibition of liquid

crystalline phases is not based on the formation of new "rod-like" or "disc-like" moieties by hydrogen-bonding, but instead on segregation due to the amphiphilic character of the glycosides, including hydrogen-bonding between the sugar heads. Carbohydrate liquid crystals experienced a fast development in the 1980's and 1990's [26-28], and the mesomorphic behaviour of new glycosides continues to be the object of systematic investigation by varying their composition and stereochemistry [30-33].

Due to its important role on the formation of liquid crystal phases, in this work we investigate with detail the hydrogen-bonding network of a natural-based glycoside, a palm kernel oil-based mannoside, αManPKO, ***1***, and its complexes with different polymeric substrates,

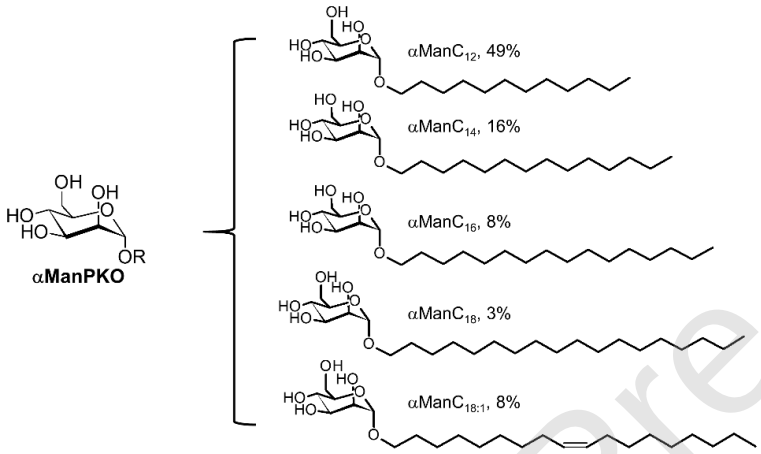

1, αManPKO

The alkyl chains of αManPKO were obtained from palm kernel oil, and then added to a mannose head by glycosidation, resulting on a mixture containing different chain lengths, and the effect of composition of *1* is currently under investigation[34]. The formation of liquid crystalline structures and its non-toxicity, makes αManPKO a promising candidate for drug delivery applications[35]. αManPKO has been complexated to three different substrates: poly(ethylene oxide), PEG, ***2***; poly(4-vinyl pyridine), P4VP, ***3***; and a block copolymer with both PEG and P4VP segments, PEG_{45}-*b*-$P4VP_{18}$, ***4***,

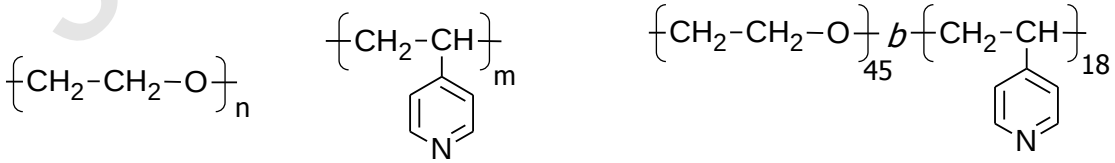

2, PEG ***3***, P4VP ***4***, PEG_{45}-*b*-$P4VP_{18}$

Whilst PEG is considered as a polymer substrate of great interest for biological applications due to its bio-compatibility[36, 37], P4VP has been widely applied as a building block to yield supramolecular polymers [13, 38-43]. Finally, block copolymers not only facilitate the introduction of new functionalities in different segments of the polymer chain, but they also offer further control over microphase separation by regulating their hydrophobic/hydrophilic ratios [44-46].

The materials are characterised by a combination of thermal, structural, spectroscopic and modelling techniques, in order to provide relevant insights on the role of the hydrogen-bonding network to assemble liquid crystalline glycosides[23]. Complexation of block-copolymers has been used for different applications and materials, including light-responsive materials studied in our lab [45]. More specifically, Ikkala and co-workers have reported several examples using P4VP as a polymeric matrix; and, for selected examples, they describe the self-assembly of P4VP block copolymers complexed with cholesteryl hemisuccinate[47] and with 3-pentadecylphenol[48]. These and other precedent works, however, focus on the structural and compositional analysis, whilst a detailed model of the hydrogen-bonding network is still crucial to describe and predict complexation. The assembly of glycosides, tackled in the present work, as well as other systems containing multiple and resonating hydrogen bonds [49], is particularly challenging, and requires accounting for several hydroxyl groups potentially acting as hydrogen-donors and hydrogen-acceptors. Our approach can then open new forefronts to prepare supramolecular liquid crystal polymers as drug-delivery and cosmetic formulations [50-54]. In the long-term, the use of amphiphilic polymers will be beneficial to provide nanocarriers stealth effects that suppress opsonisation, to reduce interactions with the reticular-endothelial system, and to ultimately prolong circulation lifetime in blood. [55-57]

2. Experimental section

Materials preparation

The mannoside αManPKO, ***1***, was synthesised according to the process described in detail in [34], and can be reviewed as electronic supplementary information (ESI, section A). D(+)-mannose monohydrate and boron trifluoride, BF_3, were purchased from Sigma Aldrich and used without further purification. The palm kernel oil, PKO, was obtained from Golden Jomalina Food Industries Sdn. Bhd. (Malaysia), and the main components after reduction were lauryl (49%), myristyl (16%) and oleyl (7%) alcohols, determined by gas chromatography-mass spectroscopy, GC-MS. The chemical structures of αManPKO and its intermediates were assessed by ^{1}H-NMR spectroscopy, using a Varian NMR Systems spectrometer at 400 MHz. D(+)-mannose was

peracetylated and PKO was reduced to alcohols, followed by glycosidation with PKO, and finally deacetylation, to yield ***1*** [35, 58, 59].

Poly(ethylene glycol), PEG, with an average molar mass of MW=12000 g·mol^{-1}, and poly(4-vinylpyridine), P4VP, with MW=60000 g·mol^{-1}, were purchased from Sigma Aldrich and used without further modification. The poly(ethylene glycol)-*b*-poly(4-vinylpyridine block copolymer, PEG_{45}-*b*-$P4VP_{18}$, was synthesised at the Institute of Materials Technology of Aragon (Zaragoza, Spain) by atom transfer radical polymerisation, and details of the synthesis and characterisation are also included as ESI (section B). The average molar mass is MW= 4350 g·mol^{-1}, and the average polymerisation degrees of each block are *n*=45 and *m*=18, verified by MALDI-TOF and ^{1}H-NMR.

The polymeric complexes were prepared by weighting appropriate amounts of αManPKO, ***1***, and the corresponding polymers (***2***, ***3*** or ***4***), in a Mettler Toledo Classic Plus digital balance (±0.01 mg), and dissolving in dichloromethane, DCM. The resulting solutions were stirred at room temperature during 24 h, and then allowed for slow evaporation during several days, until no additional weight loss was observed. Complexation was kept to 100% (full complexation), in terms of % of equivalent glycoside units respect to polymer repeating units. Three complexes were obtained, namely, PEG●αManPKO, P4VP ●αManPKO and PEG_{45}-*b*-$P4VP_{18}$●αManPKO.

Techniques and methods

The phase behaviour of αManPKO, ***1***, and the polymeric complexes ***2***, ***3*** and ***4***, was determined by polarised optical microscopy, POM, and differential scanning calorimetry, DSC. Liquid crystalline textures were assigned by using an Olympus BX51 microscope equipped with cross-polarising filters coupled to a Mettler Toledo FP82HT hot stage. Samples were sandwiched between two glass slides, heated to their respective isotropic phases, and then cooled down to room temperature, at a rate of 10°C min^{-1}. Samples for DSC were previously dried in a vacuum oven at 50°C for at least 3 hours over phosphorus pentoxide. Around 6 mg of the samples were then placed in 40 µl-sized aluminium pans, and the heat flow measured using a Mettler Toledo differential scanning calorimeter 822e, equipped with a Haake EK90/MT intercooler. Experiments were taken in subsequent heating and cooling cycles, ranging from -40°C to above their respective clearing temperatures, at rates of ±5°C min^{-1}.

The phase structures were analysed by small and wide angle X-ray diffraction, SWAXS, using a SAXess, Anton Parr, equipped with a DX-Cu 12x0.45 SERFERT X-ray tube generating CuKα radiation at λ = 1.542 Å, attached to a TCS 150 temperature controller. Samples were introduced

inside 2-cm polyimide tubes sealed with Teflon tape, and subsequently dried in a vacuum oven for at least 48 h at 30°C. Data were collected in diffraction mode and analysed with OriginPro 8 software (OriginLab). SWAXS scatterings were obtained at room temperature (T = 30°C) and then at liquid crystalline temperature (T = 120°C, 135°C, 140°C, for PEG●αManPKO, PEG_{45}-*b*-$P4VP_{18}$●αManPKO and P4VP●αManPKO, respectively), after cooling from the isotropic phase. Prior to each measurement, samples were held at the corresponding temperature for five minutes, to allow for thermal equilibration.

Temperature-dependent Fourier-transform infrared spectroscopy, FT-IR, was carried out using a Thermo Nicolet NEXUS 470 main bench (Thermo Scientific), with the sample placed in a Linkam TMS93 hot stage unit for temperature control (± 0.1K). The IR data were collected in transmittance mode and analysed with OMNIC (Thermo Scientific). Samples consisted of dispersions of the complexes into dry KBr (~1% by wt. of complex), and were prepared by grinding both components into fine powder and further compression at 200 MPa for at least 10 minutes, yielding homogeneous discs of 10 mm diameter and ~1.5 mm thickness. A pristine KBr disc was also prepared and measured as the background, immediately prior to measure the samples. Discs were heated into the isotropic phase of the complexes (above 150ºC), cooled down to room temperature, and the IR spectra were collected in isothermal steps, at 5°C intervals. Each measurement was taken after the temperature was stabilised for at least five minutes, to allow for thermal equilibration. Spectra were collected in the frequency range 4000/400 cm^{-1}, with a 4 cm^{-1} resolution, and recorded as an average of 64 scans.

Simulation Procedure

Single molecular units of $\alpha ManC_{12}$, $\alpha ManC_{18:1}$ (see chemical structure of αManPKO, ***1***), PEG, P4VP and PEG_{45}-*b*-$P4VP_{18}$ were modelled using Avogadro[60] and were optimised in Gaussian09 [61] to get a stable structure of each compound. Using *packmol*, a free modelling tool [62], a single layer of αManPKO containing $\alpha ManC_{12}$ (80% w/w) and $\alpha ManC_{18:1}$ (20% w/w), was built, with 52 C_{12} molecules and 12 $C_{18:1}$ molecules. The single layer (64 molecules total) was replicated and arranged allowing the tail groups of the lipids pointing toward each other at the centre of the bilayer and the head groups facing opposite direction to form a single bilayer. On the top and bottom of this glycoside bilayer, 32 molecules of PEG were added to form a bilayer complex. Similarly, two other bilayer systems have been built by replacing PEG with thirty-two P4VP and seven PEG_5-*b*-$P4VP_3$ chains (as a PEG_{45}-*b*-$P4VP_{18}$ model, retaining the approximate relative

composition of the block copolymer). For comparison purposes, a single bilayer of αManPKO is also modelled. The four systems were simulated using AMBER14 [63], at 303 K and 1 atm.

The four glycoside lamellar systems were then equilibrated using force field parameters from *ff99SB* [64] and *GLYCAM_06j* [65], in order to model the tails and sugar head groups of the glycolipids , respectively. The *gaff* [66] force field was used to model the PEG, P4VP and PEG_{45}-*b*-$P4VP_{18}$ systems. A non-bond cut off of 9 Å was applied in calculating non-electrostatic interactions, and the long-range electrostatic interactions were treated using the particle mesh Ewald method [67]. The SHAKE algorithm was used to constrain covalent bonds involving hydrogen. The systems were heated gradually over 2 ns from 0 to 30°C in the *NVT* ensemble, using the Andersen thermostat (τ_p =0.5 ps) and a 1 fs time step. Subsequently, the systems were equilibrated under conditions of constant pressure *NpT* by anisotropic scaling. The Berendsen algorithm was used to achieve pressure coupling, with a coupling constant of 1 ps and a compressibility of 4.5×10^{-5} bar for anisotropic coupling.

Simulations ran for a total of 350 ns, but only the last 50 ns of trajectories were used for subsequent analysis. All the coordinates were archived every 5 ps. The hydrogen bonding analysis was performed using the *cpptraj* module of AMBER, defining the O−O distance to be ≤ 4Å and an angle cut off of 120° from linearity. The local density profiles were calculated along the bilayer normal, taking the centre of the bilayer as the origin to determine the bilayer thickness. A detailed account of the methodologies is given by Manickam Achari *et al* [68].

3. Results and discussion

Phase behaviour and structure, POM, DSC and SWAXS

The phase behaviour of αManPKO and its complexes was assessed by polarised optical microscopy, POM, and confirmed by differential scanning calorimetry, DSC. αManPKO forms a monotropic smectic A phase below *ca.* 146ºC, assessed by the appearance of battonêtes under the polarised microscope, which further coalesce into a focal conic fan texture, in coexistence with homeotropic regions. The PEG●αManPKO, P4VP●αManPKO and PEG_{45}-*b*-$P4VP_{18}$●αManPKO complexes, also develop battonêtes on cooling from the isotropic melt, indicating the formation of smectic A phases below T_{SmAI}~150°C, see **Fig. 1**. These textures flash upon pressure at high temperatures, and motions cease on cooling to room temperature. These results indicate that the mesomorphism of the glycoside is transferred to the polymer complexes, and their liquid crystal phases vitrify on cooling [69-71].

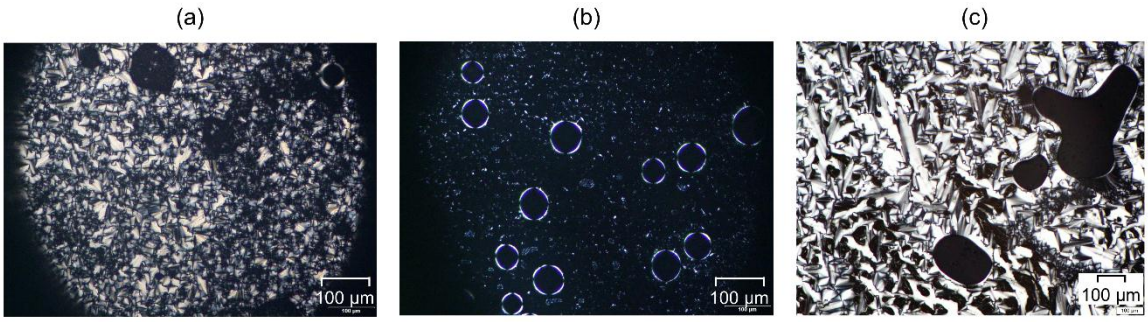

Figure 1. Polarised optical microscopy images, POM, of: (a) PEG●αManPKO, (b) P4VP●αManPKO and (c) PEG_{45}-*b*-$P4VP_{18}$●αManPKO, showing their smectic A phases at T ~ 130ºC, evolved after cooling from their isotropic phases.

The mesomorphism of the complexes is also confirmed by our DSC observations, see **Fig. 2** and **Table 1**, even though we note that the thermal transitions associated to αManPKO are weak and appear rather spread over the temperature axis. In **Fig. 2(a)**, the intense peak at T_m~60ºC indicates that the PEG chains also crystallise in the PEG●αManPKO complex, whilst in **Fig. 2(b)** the glass transition of P4VP (T_g~135ºC) is still visible in the complex, compare dotted and solid curves. These observations can be explained by the occurrence of phase separation between the polymer chains and the mannoside units.

Interestingly, it is also possible to detect a secondary glass transition at T_g~42ºC in the P4VP●αManPKO curve, **Fig. 2(b)**, which could indicate certain segregation degree of the polymer chains, with some of them undergoing a plasticizing effect by the proximity of mannoside units. Another interesting phenomenon in the P4VP●αManPKO curve is the appearance of a new melting point at T_m~13ºC, which is absent in the pristine components [34]. This temperature fits well to the melting point of dodecane and similar alkanes, and suggests that the alkyl chains of αManPKO melt in the presence of the poly(4-vinyl pyridine) chains. The previous phase transitions of the PEG and P4VP complexes are also visible in the DSC curve of PEG_{45}-*b*-$P4VP_{18}$●αManPKO, **Fig. 2(c)**, which is consistent with the occurrence of micro-segregation in block-copolymers. These transitional properties are summarised in **Fig. 2(d)**.

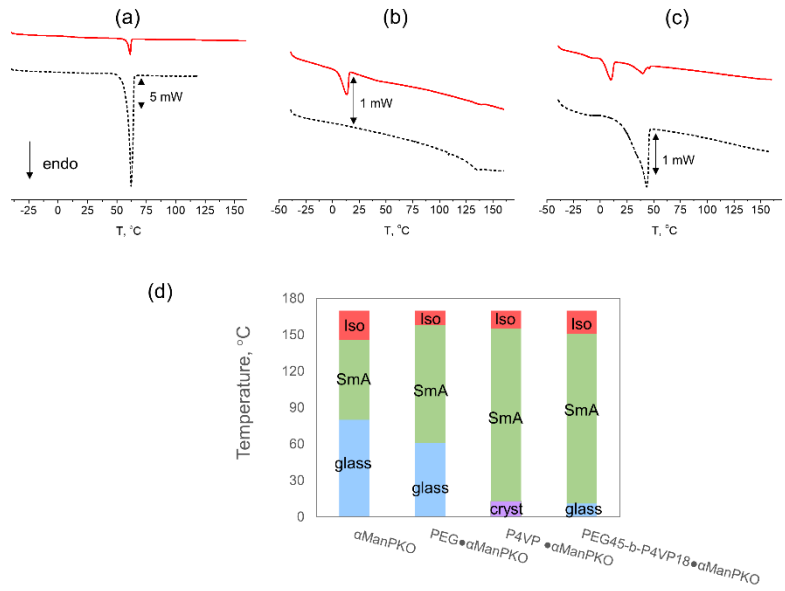

Figure 2. DSC thermograms obtained on cooling the complexes (solid curves) and the respective pristine polymers (dotted curves): (a) PEG●αManPKO and PEG; (b) P4VP●αManPKO and P4VP; and (c) PEG_{45}-*b*-$P4VP_{18}$●αManPKO and PEG_{45}-*b*-$P4VP_{18}$. Y-axis: heat flow (mW), with the curves shifted arbitrarily; (d) phase diagram of the complexes.

Table 1. Thermal transitions of the complexes and pristine mannosides obtained by differential scanning calorimetry, DSC, on cooling from the isotropic phase.

Sample	T_g (°C)	T_m (°C)	ΔH_m ($J \cdot g^{-1}$)	T_{SmAI} (°C)	ΔH_{SmAI} ($J \cdot g^{-1}$)
αManPKO	0	-	-	146	3.8
PEG	-	62	199.6	-	
P4VP	133	-	-	-	
PEG_{45}-*b*-$P4VP_{18}$	-	43	43.6	-	
PEG●αManPKO	13	61	13.0	158*	-
P4VP ●αManPKO	42 135	13	9.3	155*	-
PEG_{45}-*b*-$P4VP_{18}$●αManPKO	-9	11 39 44	10.3 2.7 0.27	151*	-

*Clearing temperatures, T_{SmAI}, were obtained from POM.

The phase structures of the complexes are now investigated by small angle X-ray scattering, SWAXS, and for each complex we now display the corresponding scatterings in **Fig. 3**, obtained at the smectic A phase (upper) and room temperature (lower), on cooling from the isotropic melt. The results are consistent with the formation of layered smectic structures, with one strong signal at low angles (d_1) and a weaker signal ($d_2 \sim d_{1/2}$), associated to first and second order signals of the smectic layer periodicities, respectively, see **Table 2**. Samples also show broad diffuse signals at wide angles, associated to the alkyl chain distances of the αManPKO molecules (d_3 ~ 4.7-4.9 Å). It is worth mentioning that PEG●αManPKO exhibits two additional sharp signals overlapping the broad region, at $d_{3'}$=3.8 Å and $d_{3''}$=4.6 Å, indicative of partial crystallisation, which is in agreement with our DSC results in **Fig. 2(a)**.

These diffractograms are essentially identical to that of pristine αManPKO and indicate the formation of smectic bilayers, d_1 ~ 31 Å, with certain degree of interdigitation of the alkyl chains (assuming an estimated averaged molecular length d *l* ~23 Å and alkyl chains found in all-*trans* configuration[34]). We note that, in the complexes, there is a slight increase in the layering spacing, which will be accounted for in terms of the molecular model developed in the next sections.

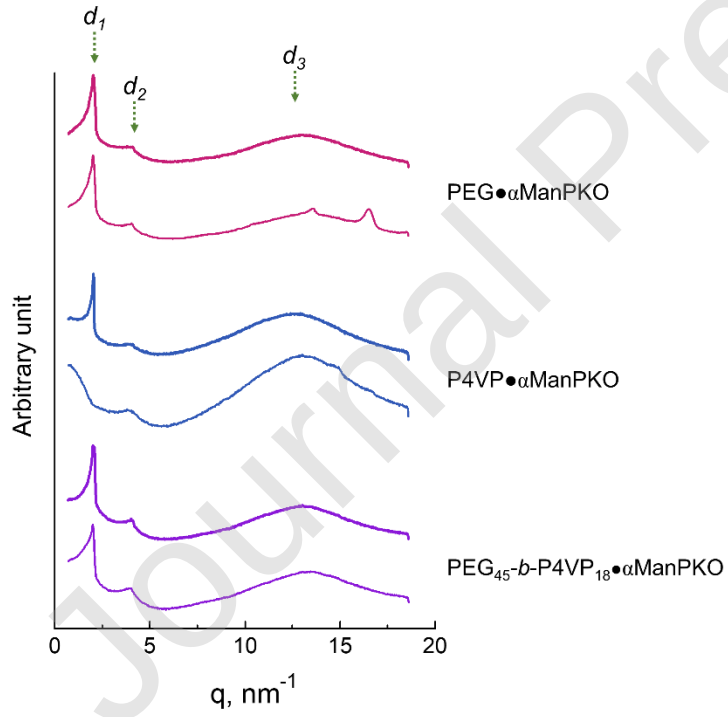

Figure 3. SWAXS scatterings of the complexes obtained in their smectic A phases (upper curves, T=140°C, 120°C and 135°C, for PEG●αManPKO, P4VP●αManPKO and PEG_{45}-*b*-$P4VP_{18}$●αManPKO, respectively) and at room temperature (lower curves, T=25°C).

Table 2. Phase structure of the polymeric complexes and αManPKO. Thickness of the bilayers/*d*-spacings (*d*, Å) as obtained by small-wide angle X-ray scattering, SWAXS.

	Glass[a]			Smectic[b]		
	d_1	d_2	d_3	d_1	d_2	d_3
αManPKO[c]	31.2	15.7	5.0	30.8	15.4	5.2
PEG●αManPKO	31.2	15.6	3.8, 4.6	30.9	15.1	4.8
P4VP●αManPKO	-	15.8	4.8	30.9	15.4	4.9
PEG_{45}-*b*-$P4VP_{18}$●αManPKO	31.3	15.6	4.7	31.2	15.6	4.8

[a]T=25°C.

[b]Smectic A phase scatterings of αManPKO, PEG●αManPKO, P4VP●αManPKO and PEG_{45}-*b*-$P4VP_{18}$●αManPKO are measured at 120°C, 120°C, 140°C and 135°C, respectively.

[c] Unpublished results[34].

Molecular interactions, FT-IR

The specific interactions responsible for the phase behaviour of αManPKO and its complexes are now investigated by temperature-dependent Fourier-transform infrared spectroscopy, FT-IR. **Fig. 4** displays the FT-IR spectra corresponding to αManPKO, PEG●αManPKO, P4VP●αManPKO and PEG_{45}-*b*-$P4VP_{18}$●αManPKO, obtained in their smectic phases, T=104°C. **Fig. 5** and **Fig. 6** highlight some specific IR vibration regions of interest.

As expected, the spectra of the complexes present several similarities, and contain different signals arising from the polymer chains and αManPKO molecules[34]. The C-C-O *st*. vibration regions of PEG and PEG●αManPKO (1300 – 900 cm^{-1}) are shown with more detail in **Fig. 5(a)** and **5(b)**, respectively, where several PEG signals (broad arrows) appear overlapped with contributions from the glycoside molecules of αManPKO, **Fig. 5(c)** (thin arrows). More specifically, the PEG●αManPKO curve in **Fig. 5(b)** shows two maxima: at 1110 cm^{-1}, from PEG, and at 1060 cm^{-1}, from αManPKO. We believe that the absence of step changes with temperature is caused by the inhibition of crystallisation of PEG in the KBr discs. The P4VP●αManPKO curve in **Fig. 6(b)**, on other hand, displays blue-shifts of the 1600 cm^{-1} peak associated to the P4VP ring vibration, **Fig. 6(a)**, which reveal the formation on cooling of new hydrogen bonds involving the pyridine ring.

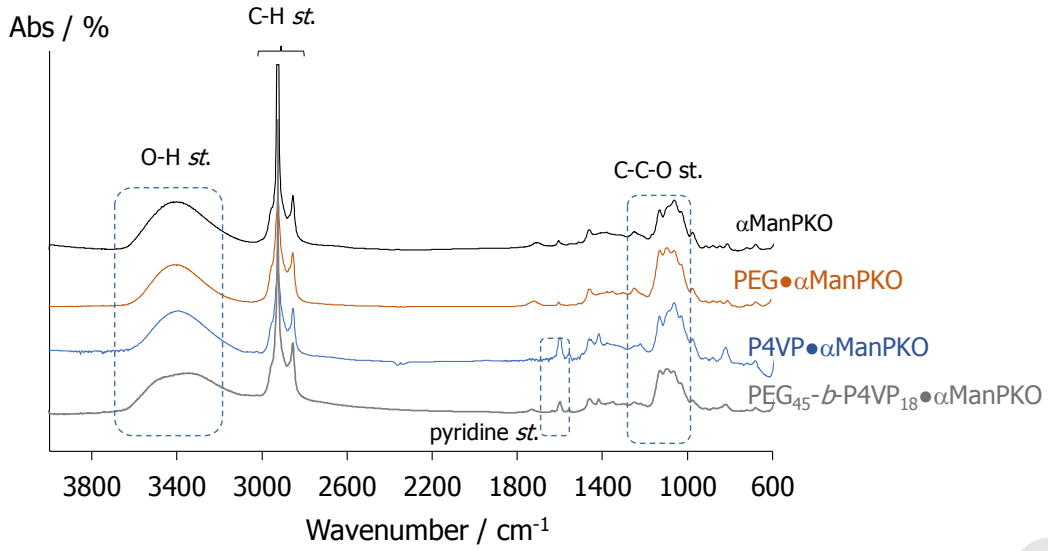

Figure 4. FT-IR spectra of the complexes and pristine αManPKO, obtained at T=104°C, highlighting some stretching, *st*., regions of interest. Curves are shifted along the Y-axis arbitrarily.

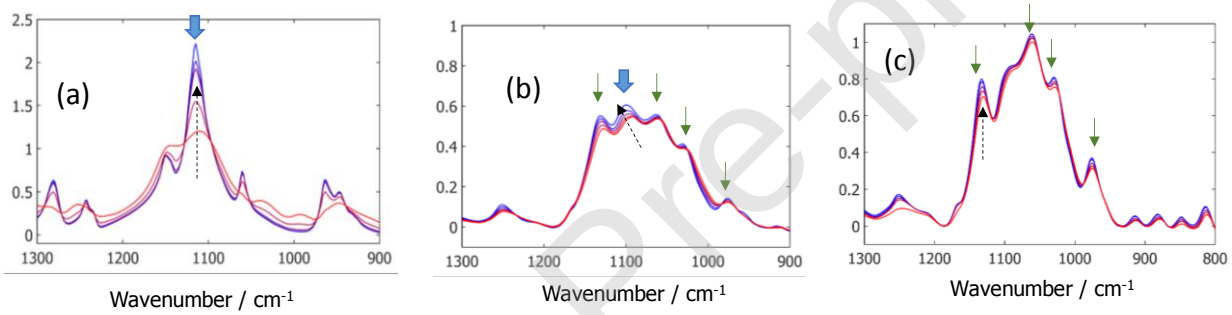

Figure 5. Temperature-dependent FT-IR spectra of (a) PEG, (b) PEG●αManPKO and (c) αManPKO, in the C-C-O *st*. region. Solid broad arrows indicate contributions from PEG, and solid narrow arrows, from αManPKO. Dotted arrows indicate the direction on cooling from the isotropic phase to room temperature; Y-axes represent IR absorbance (%).

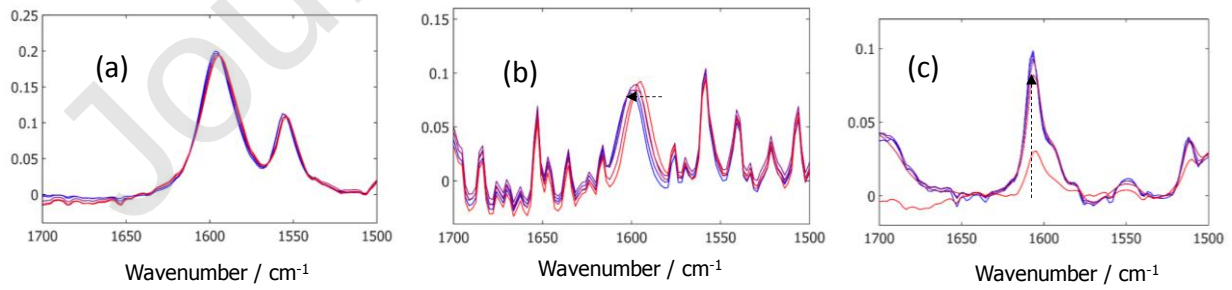

Figure 6. Temperature-dependent FT-IR spectra of (a) P4VP; (b) P4VP●αManPKO and (c) αManPKO. Dotted arrows indicate the direction on cooling from the isotropic phase to room temperature. Y-axes represent IR absorbance (%).

With the aim to investigate how potential interactions between the hydroxyl groups of αManPKO and the polymer chains can contribute to assemble the new complexes, we now analyse with detail the OH stretching regions of PEG●αManPKO and P4VP●αManPKO in **Fig. 7(a)** and **7(b)**, respectively. The broad profiles of the OH *st*. bands, typical of sugars and glycosides, denote a distribution of hydroxyl groups found in different intermolecular environments, and the relatively low wavenumbers of the signal, ν~3600-3000 cm^{-1}, confirm the presence of extensive hydrogen-bonding in these complexes[23]. The shift of the OH *st*. band towards lower frequencies on cooling indicates the progression to form stronger interactions within the hydrophilic domains of these complexes, due to the reconstruction of hydrogen bonds.

Fig. 7(c) displays the maxima of the OH stretching region as a function of the temperature, $\nu_{OH\text{-}max}$, and the values for PEG●αManPKO and P4VP●αManPKO are a few wavenumbers higher than αManPKO (at comparable temperatures), which indicates that complexation weakens the interactions between the sugar heads of the glycoside molecules of αManPKO. Interestingly, PEG_{45}-*b*-$P4VP_{18}$●αManPKO displays the opposite trend respect to αManPKO, suggesting the formation of stronger hydrogen bonds, and we will return to this observation later. The dynamic character of the hydrogen-bonding network can be semi-quantified by the slopes of the $\nu_{OH\text{-}max}$ graphs in **Fig. 7(c)**, also known as the wavenumber-temperature coefficients, WTC [72]. All samples under study, including the block copolymer, show similar values of WTC ~ 0.260 cm^{-1}/K. These also fall within the range of other sugars[72] and glycosides[23] measured in their glassy states, but are smaller than values typically obtained in liquid crystal phases. Our results are indicative of hydrogen-bonding networks with low thermal sensitivity, in terms of Angell's strength and fragility[73, 74].

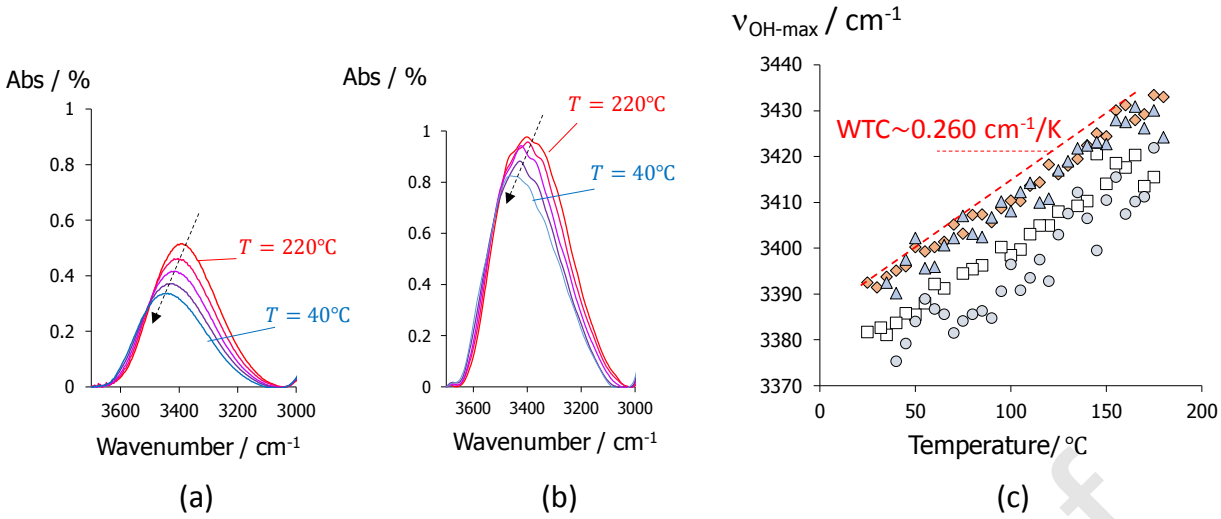

Figure 7. Temperature dependence of the IR OH stretching region corresponding to (a) PEG●αManPKO and (b) P4VP●αManPKO; (c) maxima of the OH stretching band frequency, $\nu_{OH\text{-}max}$, calculated for ◇ PEG●αManPKO, △ P4VP●αManPKO, ○ PEG_{45}-*b*-$P4VP_{18}$●αManPKO and □ αManPKO, as a function of the temperature. Dotted arrows indicate direction of the measurements on cooling.

Molecular Simulations

With the aim to assess the role of the intermolecular interactions on the phase structure of our complexes, studied in the previous sections, we have carried out molecular simulations on model systems. More specifically, we have modelled αManPKO as a mixture of mannoside molecules containing *n*=12 (C12, $\alpha ManC_{12}$ in ***1***) and *n*=18 (C18:1 with a double bond at *n*=9, $\alpha ManC_{18:1}$ in ***1***) alkyl chains, based on its average composition and in order to study the effect of unsaturation. This ratio was maintained in the simulations of the αManPKO complexes, when additional PEG and P4VP segments were included, according to the *Simulation Procedure* described above in the experimental section.

The (thickness) *d*-spacing of the bilayer was determined by calculating the local density profile, and the area per lipid of αManPKO was obtained by dividing the *xy*- plane of the bilayer with the total number of lipid present in a layer; results are shown in **Table 3**. The length of one fully stretched αManPKO molecule with single chain C12 is about 20.2 Å, while the longer hydrocarbon chain, C18:1, extends to a maximum length of 27.5 Å (with a *trans* conformation around its double bond). [68]

Snapshots of the resulting structures and conformations are displayed for PEG●αManPKO, P4VP●αManPKO, PEG_{45}-*b*-$P4VP_{18}$●αManPKO and αManPKO, in **Fig. 8(a)**, **8(b), 8(c)** and **8(d)**, respectively, and the results are in accordance with the formation of bilayers. The *d*-spacings obtained from simulations, see **Table 3**, agree with the experimental values reported above in **Table 2**. There is a slight underestimation of the layer thickness (≤11.5%), except for P4VP●αManPKO, which gives an excellent prediction with a positive +2.7% error. These deviations can be attributed to the length reduction of the complex used in simulation compared to the experimental conditions.

The *d*-spacing is always less than two times the fully stretched length of a single mannoside molecule, suggesting the adoption of *cis* conformers, favoured by the presence of the double bond between C_9—C_{10} on the C18:1 chain, which induces kinks in the linear molecular structure. Nevertheless, we must consider that interdigitation of the alkyl chains affects the *d*-spacing of the bilayers, and visual inspection of **Fig. 8(c)** and **8(d)** also hints that some chains may interdigitate between the two layers. We also note that P4VP●αManPKO shows signs of protrusion of the mannoside phase into the polymer region, see **Fig. 8(b)**. We then hypothesise that these mixing effects could be seen in the whole series if longer times were allowed, resulting in more accurate estimations of the bilayer structures.

Table 3. Calculated (modelled) thickness (*d*-spacing) of bilayers and area per lipid *A* / $Å^2$.

Complexes modelled	*d*-spacing (Å)	Area per lipid, *A*($Å^2$)
PEG●αManPKO	28.7 ± 0.8	31.7 ± 0.2
P4VP●αManPKO	31.6 ± 0.2	24.1 ± 0.4
PEG_{45}-*b*-$P4VP_{18}$●αManPKO	27.7 ± 0.6	29.9 ± 0.3
αManPKO	29.6 ± 0.8	35.4 ± 0.5

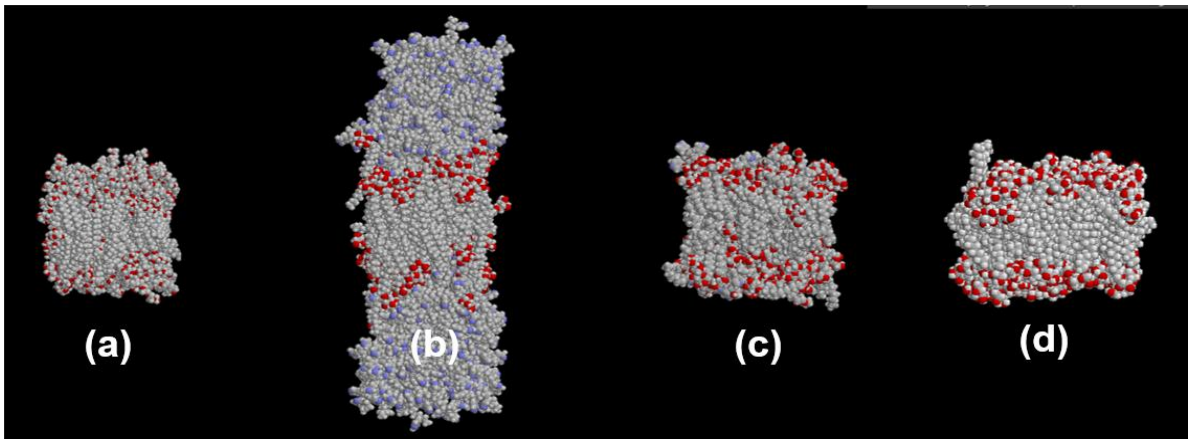

Figure 8. Snapshots of the molecular models used for (a) PEG●αManPKO, (b) P4VP●αManPKO, (c) PEG_{45}-*b*-$P4VP_{18}$●αManPKO and (d) αManPKO.

The FT-IR results have already evidenced the formation of specific interactions between the mannoside molecules and the respective polymer chains in the complexes, and we now quantify hydrogen-bonding *via* our molecular simulations. Based on previous findings[34, 75], we can rule out relevant intramolecular effects, and we then focus on intermolecular hydrogen-bonding between constituents moieties. **Fig. 9** illustrates the hydroxyl groups at the αManPKO sugar heads capable to form hydrogen bonds, namely, O1H, O2H, O3H and O5H, and we note that these can act as both hydrogen donors and acceptors. PEG and P4VP segments contain hydrogen acceptors (oxygen and nitrogen atoms, respectively), and PEG segments also contain hydrogen donors (terminal hydroxyl groups, see **Fig. ESI7**).

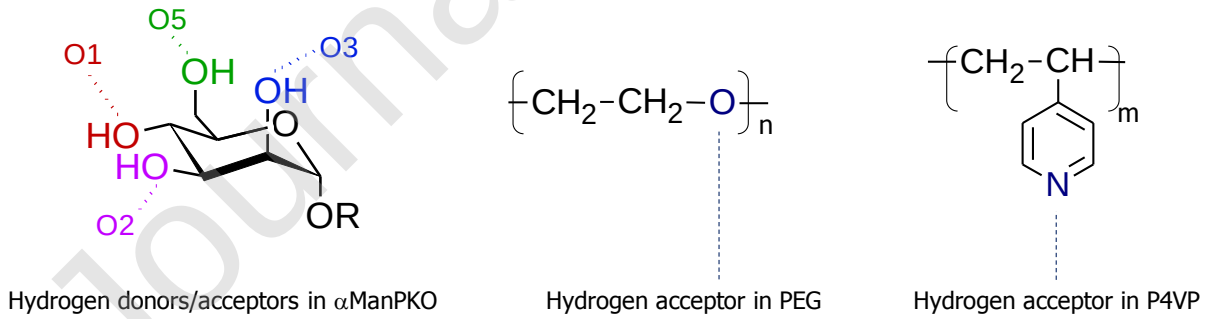

Figure 9. Labelling of the groups acting as hydrogen donors/acceptors in the complexes. We note that OH residual groups exist in both the PEG (O21, O28) and PEG_{45}-*b*-$P4VP_{18}$ (O201, O208) segments used during simulations, according to **Tables ESI3** and **ESI4**, and **Fig. ESI7**.

Table 4 summarises the hydrogen bonds (hits) formed in the bilayer complexes of our PEG●αManPKO, P4VP●αManPKO, PEG_{45}-*b*-$P4VP_{18}$●αManPKO and αManPKO models. The total number of hydrogen bonds between glycosides (C12 and C18:1) fall between 99 to 111 hit per-frame, with an average of 106 hit per-frame, and this indicates that the interactions between glycosides are not extensively modified by the presence and nature of polymer chains at the hydrophilic interlayer region, at least for pristine PEG and P4VP. Indeed, glycosides predominantly form hydrogen bonds *via* the equatorial O1 hydroxyl group, regardless of the presence and nature of the polymer chain.

Hydrogen-bonding between glycosides and the polymer chains does show some significant differences. In terms of overall interactions, the glycosides form more hydrogen bonds with PEG (52) than with P4VP (31), and the PEG segments preferentially form new hydrogen bonds with glycosides, rather than within other CH_2CH_2O groups in the PEG chain, see 13.92 + 2.57 > 11.18 in **Table ESI3** (O21 and O28). By comparing the C12/C18:1-PEG and C12/C18:1-P4VP totals in **Table 4(a)** and **4(b)**, there seems to be a stronger tendency for C18:1 molecules to interact with P4VP than with PEG, and this can be also seen from **Table 4(c)** for PEG_{45}-*b*-$P4VP_{18}$●αManPKO. These results cannot be explained, at least solely, by differences in hydrogen-bonding strength, since the $\nu_{OH\text{-}max}$ (and WTC) values for PEG●αManPKO and P4VP●αManPKO in **Fig. 7(c)** almost overlap. Interactions must be then favoured by a stronger interfacial mixing of PEG chains and mannoside molecules at the bilayer boundaries, due to the hydrophilic nature of the PEG chains. In the case of P4VP, such interfacial interactions must be somehow hindered by the more hydrophobic nature of the pyridine ring, probably coupled with steric effects, and perhaps offset by the stereochemistry of C18:1.

Interestingly, the PEG_{45}-*b*-$P4VP_{18}$●αManPKO model provides different tendencies for hydrogen-bonding respect to the pristine polymers, see **Table 4(c)**. As a first observation, the O2H group in the mannoside tends to form more hydrogen bonds than O1H, and P4VP is now the preferred polymer segment to interact with the glycosides, respect to PEG (8.464 > 6.121 in the total columns). These changes in the local distribution of hydrogen bonding could be favoured by a better interfacial mixing between polymer chains and glycosides bilayers, due to the amphiphilic character of the block-copolymer. As a result, the pyridine group of P4VP is capable to form stronger interactions with the hydroxyl groups of αManPKO than PEG[4], which is in excellent agreement with the shift to lower frequencies in the IR OH stretching band of PEG_{45}-*b*-$P4VP_{18}$●αManPKO reported above in **Fig. 7(c)**.

Table 4(a). Hydrogen-bonding hits per frame, corresponding to the PEG●αManPKO model. First molecular unit acts as donor, second as acceptor (for example, in C12 – PEG, C12 is the hydrogen donor, and the PEG unit the hydrogen acceptor). Oxygen notation according to Fig. 9 and Fig. ESI7.

	C12-C12	C12-C18:1	C18:1-C18:1	C18:1-C12	Total	C12-PEG	C18:1-PEG	Total
O1	18.14	5.59	2.81	3.54	**30.07**	13.07	2.87	**76.08**
O2	17.85	4.11	1.88	4.11	**27.96**	13.99	2.50	**72.41**
O3	17.98	2.69	2.24	3.63	**26.54**	10.69	2.47	**66.25**
O5	13.47	1.84	2.09	1.71	**19.11**	5.41	1.03	**44.65**
Total	67.44	14.23	9.02	12.99	**103.68**	43.16	8.87	**52.03**

Table 4(b). Hydrogen-bonding hits per frame corresponding to the P4VP●αManPKO model.

	C12-C12	C12-C18:1	C18:1-C18:1	C18:1-C12	Total	C12- P4VP	C18:1-P4VP	Total
O1	18.45	7.94	0.02	6.80	**33.21**	6.29	4.09	**10.37**
O2	16.85	7.03	0.85	6.06	**30.79**	5.75	0.57	**6.32**
O3	19.20	3.58	2.86	2.30	**27.94**	6.38	2.76	**9.14**
O5	14.75	1.51	1.88	0.31	**18.45**	4.37	1.24	**5.60**
Total	69.25	20.06	5.61	15.47	**110.39**	22.78	8.65	**31.43**

Table 4(c). Hydrogen-bonding hits per frame corresponding to the PEG_{45}-*b*-$P4VP_{18}$●αManPKO model.

	C12-C12	C12-C18:1	C18:1-C18:1	C18:1-C12	Total	C12-PEG	C18:1-PEG	Total	C12-P4VP	C18:1-P4VP	Total
O1	20.89	3.01	1.61	6.01	**31.52**	1.296	0.840	**2.136**	2.878	0.0004	2.878
O2	24.82	3.51	0.69	5.25	**34.27**	1.476	0.257	**1.732**	2.807	0.0000	2.807
O3	18.41	4.10	1.81	3.47	**27.79**	1.286	0.037	**1.323**	1.906	0.0000	1.906
O5	13.04	0.75	1.35	0.86	**16.00**	0.906	0.025	**0.930**	0.874	0.0000	0.874
Total	77.16	11.37	5.47	15.58	**109.59**	4.963	1.158	**6.121**	8.464	0.0004	**8.464**

Table 4(d). Hydrogen-bonding hits per frame corresponding to the αManPKO model.

	C12-C12	C12-C18:1	C18:1-C18:1	C18:1-C12	Total
O1	20.41	4.82	2.26	3.89	**31.38**
O2	15.98	2.32	2.70	1.88	**22.88**
O3	18.37	3.94	2.33	2.33	**26.97**
O5	12.69	2.68	1.12	2.18	**18.66**
Total	67.45	13.76	8.41	10.28	**99.90**

Conclusions

We have prepared complexes of the so-called αManPKO mannoside with different polymeric substrates, resulting in three new supramolecular polymers with smectic A mesomorphism, following a facile method to yield new formulations containing natural-based liquid crystal carbohydrates, and their lyotropic properties in water solutions are under current evaluation. The polymeric segments are located at the interface of glycoside bilayers, stabilised by specific interactions with the αManPKO molecules.

The interfacial miscibility between the poly(ethylene oxide) segments and the mannosides promotes hydrogen-bonding in the PEG●αManPKO complex, whilst low solubility and steric effects may restrict the interactions involving the poly(4-vynil pyridine) chains and αManPKO in the P4VP●αManPKO complex. Alternatively, the amphiphilic character of the PEG_{45}-b-$P4VP_{18}$ block-copolymer seems to facilitate the interactions of the glycosides with the P4VP units in the PEG_{45}-b-$P4VP_{18}$●αManPKO complex. Hence, it is possible to establish stronger hydrogen-bonding with the mannoside molecules, due to the high hydrogen acceptor character of the pyridine ring.

The detailed experimental/modelling analysis of the hydrogen bonds allows to discriminate interactions between different components and hydrogen acceptors and donors within sugar heads, thus opening new strategies to modify the properties of glycosides by tuning and monitoring the hydrogen-bonding network. We plan to extent this methodology to calculate the interactions using other glycosides and varying the relative block sizes, and to introduce new functionalities (such as light-responsive molecules) in different polymer blocks capable to simultaneously yield strong hydrogen bonds and favourable interfacial mixing.

Credit author statement

Nurul Fadhilah Kamalul Aripin. Conceptualization, Data curation, Data curation, Writing - original draft, Writing - review & editing, Funding acquisition.

Jonathan Heap. Experimental work, Data curation, Formal analysis.

Rafael Piñol. Experimental work, Data curation, Methodology.

Vijayan M. Achari. Data curation, Formal analysis, Writing - original draft.

Alfonso Martinez-Felipe. Conceptualization, Investigation, Writing - original draft, Writing - review & editing, Funding acquisition.

Declaration of interests

The authors declare that they have no known competing financial interests or personal relationships that could have appeared to influence the work reported in this paper.

Acknowledgements

This work was supported by the Ministry of Education of Malaysia [FRGS/1/2019/TK05/UITM/02/9, 2019]; Royal Academy of Engineering, U.K., and Academy of Science, Malaysia [NRCP1516/4/61, 2016]; University of Aberdeen [SF10192, 2018] and University Malaya [UMRG grant RP038B-17AFR].

References

1. Martinez-Felipe A, Cook AG, Abberley JP, Walker R, Storey JMD, Imrie CT. An FT-IR spectroscopic study of the role of hydrogen bonding in the formation of liquid crystallinity for mixtures containing bipyridines and 4-pentyloxybenzoic acid. Rsc Advances 2016;6:108164-79.

2. Martinez-Felipe A, Imrie CT. The role of hydrogen bonding in the phase behaviour of supramolecular liquid crystal dimers. J Mol Struct 2015 11/15;1100:429-37.

3. Ferlay S, Hosseini MW. Molecular tectonics: Design of hybrid networks and crystals based on charge-assisted hydrogen bonds. In: C. F. Samori, editor. Functional supramolecular architectures for organic electronics and nanotechnology vol. 1. . Weinheim: Wiley-VCH; 2011. .

4. Martinez-Felipe A, Brebner F, Zaton D, Concellon A, Ahmadi S, Pinol M, Oriol L. Molecular recognition via hydrogen bonding in supramolecular complexes: A fourier transform infrared spectroscopy study. Molecules 2018 SEP;23(9):2278.

5. Kato T, Frechet JMJ. New approach to mesophase stabilization through hydrogen-bonding molecular-interactions in binary-mixtures. Journal of the American Chemical Society 1989 Oct 25;111(22):8533-4.

6. Kato T, Wilson PG, Fujishima A, Frechet JMJ. Hydrogen-bonded liquid-crystals - a novel mesogen incorporating nonmesogenic 4,4'-bipyridine through selective recognition between hydrogen-bonding donor and acceptor. Chem Lett 1990 NOV 1990(11):2003-6.

7. Willis K, Price DJ, Adams H, Ungar G, Bruce DW. Hydrogen-bonded liquid crystals from alkoxystilbazoles and 3-cyanophenols: Structural control of mesomorphism. molecular structure of the complex between 4-cyanophenol and 4-octyloxystilbazole. Journal of Materials Chemistry 1995 DEC 1995;5(12):2195-9.

8. Price D, Willis K, Richardson T, Ungar G, Bruce D. Hydrogen bonded liquid crystals from nitrophenols and alkoxystilbazoles. Journal of Materials Chemistry 1997 JUN;7(6):883-91.

9. Wong JP, Whitwood AC, Bruce DW. Hydrogen-bonded complexes between 4-alkoxystilbazoles and fluorophenols: Solid-state structures and liquid crystallinity. Chemistry-a European Journal 2012 DEC;18(50):16073-89.

10. Gimeno N, Ros MB, Serrano JL, de la Fuente MR. Hydrogen-bonded banana liquid crystals. Angewandte Chemie-International Edition 2004 2004;43(39):5235-8.

11. Perez A, Gimeno N, Vera F, Ros MB, Serrano JL, De la Fuente MR. New H-bonded complexes and their supramolecular liquid-crystalline organizations. European Journal of Organic Chemistry 2008 FEB 2008(5):826-33.

12. Vapaavuori J, Bazuin CG, Priimagi A. Supramolecular design principles for efficient photoresponsive polymer-azobenzene complexes. Journal of Materials Chemistry C 2018 MAR 7;6(9):2168-88.

13. Priimagi A, Cattaneo S, Ras RHA, Valkama S, Ikkala O, Kauranen M. Polymer-dye complexes: A facile method for high doping level and aggregation control of dye molecules. Chemistry of Materials 2005 NOV 15 2005;17(23):5798-802.

14. Saccone M, Pfletscher M, Dautzenberg E, Dong RY, Michal CA, Giese M. Hydrogen-bonded liquid crystals with broad-range blue phases. Journal of Materials Chemistry C 2019 MAR 21;7(11):3150-3.

15. Walker R, Pociecha D, Abberley JP, Martinez-Felipe A, Paterson DA, Forsyth E, Lawrence GB, Henderson PA, Storey JMD, Gorecka E, et al. Spontaneous chirality through mixing achiral components: A twist-bend nematic phase driven by hydrogen-bonding between unlike components. Chemical Communications 2018 APR 7;54(27):3383-6.

16. Paterson DA, Martinez-Felipe A, Jansze SM, Marcelis ATM, Storey JMD, Imrie CT. New insights into the liquid crystal behaviour of hydrogen-bonded mixtures provided by temperature-dependent FTIR spectroscopy. Liquid Crystals 2015;5-6:928-39.

17. Jansze SM, Martinez-Felipe A, Storey JMD, Marcelis ATM, Imrie CT. A twist-bend nematic phase driven by hydrogen bonding. Angewandte Chemie-International Edition 2015 JAN 7 2015;54(2):643-6.

18. Vanti L, Mohd Alauddin S, Zaton D, Aripin NFK, Giacinti-Baschetti M, Imrie CT, Ribes-Greus A, Martinez-Felipe A. Ionically conducting and photoresponsive liquid crystalline terpolymers: Towards multifunctional polymer electrolytes. European Polymer Journal 2018 December 2018;109:124-32.

19. Mulder D, Liang T, Xu Y, ter Schiphorst J, Scheres LMW, Oosterlaken BM, Borneman Z, Nijmeijer K, Schenning APHJ. Proton conductive cationic nanoporous polymers based on smectic liquid crystal hydrogen-bonded heterodimers. Journal of Materials Chemistry C 2018 MAY 14;6(18):5018-24.

20. Martinez-Felipe A, Imrie CT, Ribes-Greus A. Study of structure formation in side-chain liquid crystal copolymers by variable temperature fourier transform infrared spectroscopy. Industrial & Engineering Chemistry Research 2013 Jul 3;52(26):8714-21.

21. Fischer E, Helferich B. New synthetic glucoside. Justus Liebigs Ann Chem 1911 1911;383(1/3):68-91.

22. Noller CR, Rockwell WC. The preparation of some higher alkylglucosides. J Am Chem Soc 1938 09/01;60(9):2076-7.

23. Cook AG, Martinez-Felipe A, Brooks NJ, Seddon JM, Imrie CT. New insights into the transitional behaviour of methyl-6-O-(n-dodecanoyl)-alpha-D-glucopyranoside using variable temperature FTIR spectroscopy and X-ray diffraction. Liquid Crystals 2013 DEC 1 2013;40(12):1817-27.

24. Cook AG, Wardell JL, Imrie CT. Carbohydrate liquid crystals: Synthesis and characterisation of the methyl-6-O-(n-acyl)-alpha-D-glucopyranosides. Chem Phys Lipids 2011 FEB 2011;164(2):118-24.

25. Cook AG, Wardell JL, Brooks NJ, Seddon JM, Martinez-Felipe A, Imrie CT. Non-symmetric liquid crystal dimer containing a carbohydrate-based moiety. Carbohydrate Research 2012 Oct 1;360:78-83.

26. Jeffrey GA, Bhattacharjee S. Carbohydrate liquid-crystals .2. Carbohydr Res 1983 1983;115(APR):53-8.

27. Jeffrey GA. Carbohydrate liquid-crystals. Acc Chem Res 1986 JUN 1986;19(6):168-73.

28. Jeffrey GA, Wingert LM. Carbohydrate liquid-crystals. Liquid Crystals 1992 Aug;12(2):179-202.

29. Praefcke K, Kohne B, Diele S, Pelzl G, Kjaer A. Mesophase characterization of some long-chain vicinal multihydroxy amphiphiles [1,2]. Liquid Crystals 1992 JAN 1992;11(1):1-8.

30. Liew CY, Salim M, Zahid NI, Hashim R. Biomass derived xylose guerbet surfactants: Thermotropic and lyotropic properties from small-angle X-ray scattering. Rsc Advances 2015;5(120):99125-32.

31. Patrick M, Zahid NI, Kriechbaum M, Hashim R. Guerbet glycolipids from mannose: Liquid crystals properties. Liquid Crystals 2018 DEC 8;45(13-15):1970-86.

32. Hashim R, Zahid NI, Velayutham TS, Aripin NFK, Ogawa S, Sugimura A. Dry thermotropic glycolipid self-assembly: A review. Journal of Oleo Science 2018 JUN;67(6):651-68.

33. Hashim R, Hashim HHA, Rodzi NZM, Hussen RSD, Heidelberg T. Branched chain glycosides: Enhanced diversity for phase behavior of easily accessible synthetic glycolipids. Thin Solid Films 2006 JUN 19;509(1-2):27-35.

34. Martinez-Felipe A, Farquharson E, Hashim R, Velayutham TS, Aripin NFK. Glycolipids from natural sources: Dry liquid crystal properties, hydrogen bonding and molecular mobility of palm kernel oil mannosides. Liquid Crystals 2019, submitted.

35. Aripin NFK, Park JW, Park HJ. Preparation of vesicle drug carrier from palm oil- and palm kernel oil-based glycosides. Colloids and Surfaces B-Biointerfaces 2012 JUN 15 2012;95:144-53.

36. Jeong B, Kim S, Bae Y. Thermosensitive sol-gel reversible hydrogels. Adv Drug Deliv Rev 2002 JAN 17;54(1):37-51.

37. Allen C, Han J, Yu Y, Maysinger D, Eisenberg A. Polycaprolactone-b-poly(ethylene oxide) copolymer micelles as a delivery vehicle for dihydrotestosterone. J Controlled Release 2000 FEB 3;63(3):275-86.

38. Stewart D, Imrie CT. Supramolecular side-chain liquid-crystal polymers .1. thermal-behavior of blends of a low molar-mass mesogenic acid and amorphous polymers. Journal of Materials Chemistry 1995 Feb;5(2):223-8.

39. Craig A, Imrie C. Side-chain liquid crystal copolymers containing nonmesogenic units: Dependence of the thermal behavior upon composition. Journal of Polymer Science Part A-Polymer Chemistry 1996 FEB;34(3):421-8.

40. Stewart D, Imrie C. Synthesis and characterization of spin-labelled and spin-probed side-chain liquid crystal polymers. Polymer 1996 JUL;37(15):3419-25.

41. Stewart D, Paterson BJ, Imrie CT. Towards supramolecular side-chain liquid crystal polymers .4. blends of low molar mass mesogens with amorphous polymers. European Polymer Journal 1997 Mar;33(3):285-90.

42. Saccone M, Dichiarante V, Forni A, Goulet-Hanssens A, Cavallo G, Vapaavuori J, Terraneo G, Barrett CJ, Resnati G, Metrangolo P, et al. Supramolecular hierarchy among halogen and hydrogen bond donors in light-induced surface patterning. Journal of Materials Chemistry C 2015;3(4):759-68.

43. Ikkala O, ten Brinke G. Hierarchical self-assembly in polymeric complexes: Towards functional materials. Chemical Communications 2004(19):2131-7.

44. Concellon A, Claveria-Gimeno R, Velazquez-Campoy A, Abian O, Pinol M, Oriol L. Polymeric micelles from block copolymers containing 2,6-diacylaminopyridine units for encapsulation of hydrophobic drugs. Rsc Advances 2016;6(29):24066-75.

45. Concellon A, Blasco E, Martinez-Felipe A, Carlos Martinez J, Sics I, Ezquerra TA, Nogales A, Pinol M, Oriol L. Light-responsive self-assembled materials by supramolecular post-functionalization via hydrogen bonding of amphiphilic block copolymers. Macromolecules 2016 OCT 25;49(20):7825-36.

46. Concellon A, Blasco E, Pinol M, Oriol L, Diez I, Berges C, Sanchez-Somolinos C, Alcala R. Photoresponsive polymers and block copolymers by molecular recognition based on multiple hydrogen bonds. Journal of Polymer Science Part A-Polymer Chemistry 2014 NOV 15 2014;52(22):3173-84.

47. Korhonen JT, Verho T, Rannou P, Ikkala O. Self-assembly and hierarchies in pyridine-containing homopolymers and block copolymers with hydrogen-bonded cholesteric side-chains. Macromolecules 2010 FEB 9 2010;43(3):1507-14.

48. Valkama S, Ruotsalainen T, Nykanen A, Laiho A, Kosonen H, ten Brinke G, Ikkala O, Ruokolainen J. Self-assembled structures in diblock copolymers with hydrogen-bonded amphiphilic plasticizing compounds. Macromolecules 2006 DEC 26;39(26):9327-36.

49. Saccone M, Pfletscher M, Kather S, Woelper C, Daniliuc C, Mezger M, Giese M. Improving the mesomorphic behaviour of supramolecular liquid crystals by resonance-assisted hydrogen bonding. Journal of Materials Chemistry C 2019 JUL 28;7(28):8643-8.

50. Brienne MJ, Gabard J, Lehn JM, Stibor I. Macroscopic expression of molecular recognition - supramolecular liquid-crystalline phases induced by association of complementary heterocyclic components. Journal of the Chemical Society-Chemical Communications 1989 Dec 15(24):1868-70.

51. Lehn JM. Perspectives in supramolecular chemistry - from molecular recognition towards molecular information-processing and self-organization. Angewandte Chemie-International Edition in English 1990 Nov;29(11):1304-19.

52. Krische MJ, Lehn JM. The utilization of persistent H-bonding motifs in the self-assembly of supramolecular architectures. Molecular Self-Assembly: Organic Versus Inorganic Approaches 2000 2000;96:3-29.

53. Kolesnichenko IV, Anslyn EV. Practical applications of supramolecular chemistry. Chem Soc Rev 2017 MAY 7;46(9):2385-90.

54. Amabilino DB, Smith DK, Steed JW. Supramolecular materials. Chem Soc Rev 2017 MAY 7;46(9):2404-20.

55. Pasut G, Paolino D, Celia C, Mero A, Joseph AS, Wolfram J, Cosco D, Schiavon O, Shen H, Fresta M. Polyethylene glycol (PEG)-dendron phospholipids as innovative constructs for the preparation of super stealth liposomes for anticancer therapy. J Controlled Release 2015 FEB 10;199:106-13.

56. Pippa N, Naziris N, Stellas D, Massala C, Zouliati K, Pispas S, Demetzos C, Forys A, Marcinkowski A, Trzebicka B. PEO-b-PCL grafted niosomes: The cooperativilty of amphiphilic components and their properties in vitro and in vivo. Colloids and Surfaces B-Biointerfaces 2019 MAY 1;177:338-45.

57. Paolino D, Cosco D, Licciardi M, Giammona G, Fresta M, Cavallaro G. Polyaspartylhydrazide copolymer-based supramolecular vesicular aggregates as delivery devices for anticancer drugs. Biomacromolecules 2008 APR;9(4):1117-30.

58. NYSTROM R, BROWN W. Reduction of organic compounds by lithium aluminum hydride .1. aldehydes, ketones, esters, acid chlorides and acid anhydrides. J Am Chem Soc 1947;69(5):1197-9.

59. Polakova M, Belanova M, Petrus L, Mikusova K. Synthesis of alkyl and cycloalkyl alpha-D-mannopyranosides and derivatives thereof and their evaluation in the mycobacterial mannosyltransferase assay. Carbohydr Res 2010 JUL 2;345(10):1339-47.

60. Hanwell MD, Curtis DE, Lonie DC, Vandermeersch T, Zurek E, Hutchison GR. Avogadro: An advanced semantic chemical editor, visualization, and analysis platform. Journal of Cheminformatics 2012 AUG 13;4:17.

61. Gaussian I. Gaussian 09, Revision A.02 [computer program]. Wallingford CT: 2016. .

62. Martinez L, Andrade R, Birgin EG, Martinez JM. PACKMOL: A package for building initial configurations for molecular dynamics simulations. Journal of Computational Chemistry 2009 OCT;30(13):2157-64.

63. Case A, Babin V, Berryman JT, Betz RM, Cai Q, Cerutti DS, Cheatham I, T.E., Darden TA, Duke RE, Gohlke H, et al. AMBER [computer program]. San Francisco: University of California; 2014. .

64. Maier JA, Martinez C, Kasavajhala K, Wickstrom L, Hauser KE, Simmerling C. ff14SB: Improving the accuracy of protein side chain and backbone parameters from ff99SB. Journal of Chemical Theory and Computation 2015 AUG;11(8):3696-713.

65. Kirschner KN, Lins RD, Maass A, Soares TA. A glycam-based force field for simulations of lipopolysaccharide membranes: Parametrization and validation. Journal of Chemical Theory and Computation 2012 NOV;8(11):4719-31.

66. Wang J, Wang W, Kollman PA, Case DA. Automatic atom type and bond type perception in molecular mechanical calculations. Journal of Molecular Graphics & Modelling 2006 OCT;25(2):247-60.

67. DARDEN T, YORK D, PEDERSEN L. Particle mesh ewald - an N.log(n) method for ewald sums in large systems. J Chem Phys 1993 JUN 15;98(12):10089-92.

68. Achari VM, Nguan HS, Heidelberg T, Bryce RA, Hashim R. Molecular dynamics study of anhydrous lamellar structures of synthetic glycolipids: Effects of chain branching and disaccharide headgroup. J Phys Chem B 2012 SEP 27;116(38):11626-34.

69. Kocherbitov V, Soderman O. Glassy crystalline state and water sorption of alkyl maltosides. Langmuir 2004 APR 13;20(8):3056-61.

70. Ericsson C, Ericsson L, Kocherbitov V, Soderman O, Ulvenlund S. Thermotropic phase behaviour of long-chain alkylmaltosides. Physical Chemistry Chemical Physics 2005;7(15):2970-7.

71. Ogawa S, Asakura K, Osanai S. Thermotropic and glass transition behaviors of n-alkyl beta-D-glucosides. Rsc Advances 2013;3(44):21439-46.

72. Wolkers WF, Oliver AE, Tablin F, Crowe JH. A fourier-transform infrared spectroscopy study of sugar glasses. Carbohydr Res 2004 APR 28 2004;339(6):1077-85.

73. ANGELL C. Formation of glasses from liquids and biopolymers. Science 1995 MAR 31;267(5206):1924-35.

74. ANGELL C. Relaxation in liquids, polymers and plastic crystals - strong fragile patterns and problems. J Non Cryst Solids 1991 JUN;131:13-31.

75. Kotena ZM, Behjatmanesh-Ardakani R, Hashim R. AIM and NBO analyses on hydrogen bonds formation in sugar-based surfactants (alpha/beta-d-mannose and n-octyl-alpha/beta-d-mannopyranoside): A density functional theory study. Liquid Crystals 2014 JUN 3;41(6):784-92.